JOURNAL OF GEOPHYSICAL RESEARCH, VOL. 114, D04111, doi:10.1029/2008JD010825, 2009

Stable water isotopes in HadCM3: Isotopic signature of El Niño–Southern Oscillation and the tropical amount effect

J. C. Tindall,[1] P. J. Valdes,[1] and L. C. Sime[2]

Received 22 July 2008; revised 12 October 2008; accepted 21 November 2008; published 21 February 2009.

[1] Stable water isotopes have been added to the full hydrological cycle of the Hadley Centre Climate model (HadCM3) coupled atmosphere-ocean GCM. Simulations of $\delta^{18}O$ in precipitation and at the ocean surface compare well with observations for the present-day climate. The model has been used to investigate the isotopic anomalies associated with ENSO; it is found that the anomalous $\delta^{18}O$ in precipitation is correlated with the anomalous precipitation amount in accordance with the "amount effect." The El Niño $\delta^{18}O$ anomaly at the ocean surface is largest in coastal regions because of the mixing of ocean water and the more depleted runoff from the land surface. Coral $\delta^{18}O$ anomalies were estimated, using an established empirical relationship, and generally reflect ocean surface $\delta^{18}O$ anomalies in coastal regions and sea surface temperatures away from the coast. The spatial relationship between tropical precipitation and $\delta^{18}O$ was investigated for the El Niño anomaly simulated by HadCM3. Weighting the El Niño precipitation anomaly by the precipitation amount at each grid box gave a large increase in the spatial correlation between tropical precipitation and $\delta^{18}O$. This improvement was most apparent over land points and between 10 and 20° of latitude.

Citation: Tindall, J. C., P. J. Valdes, and L. C. Sime (2009), Stable water isotopes in HadCM3: Isotopic signature of El Niño–Southern Oscillation and the tropical amount effect, *J. Geophys. Res.*, *114*, D04111, doi:10.1029/2008JD010825.

1. Introduction

[2] Stable water isotopes ($H_2^{18}O$ and $HD^{16}O$) have been used for many years to infer information about climate both past and present. Isotopic information can be used to make inferences about temperature, precipitation, or circulation patterns [e.g., *Dansgaard et al.*, 1993]. Stable water isotopes were first incorporated into the hydrological cycle of a General Circulation Model (GCM) by *Joussaume et al.* [1984] and have since been included in the hydrological cycle of several other GCMs [e.g., *Hoffmann et al.*, 1998; *Mathieu et al.*, 2002; *Noone and Simmonds*, 2002; *Lee et al.*, 2007] in order to help interpret isotopes in paleoproxies [e.g., *Werner et al.*, 2001; *Vuille et al.*, 2003; *Noone*, 2008] and to enable more accurate model data comparison. Most of these GCMs have only considered the atmospheric component of the model and have prescribed sea surface temperature and sea surface isotope values. However stable water isotopes have been incorporated into the GISS coupled atmosphere-ocean GCM [*Schmidt*, 1998], and that model is now able to investigate paleoclimate events such as the 8.2 ka event [*LeGrande et al.*, 2006]. As part of the ISOMAP-UK project, stable water isotopes have been incorporated into the full hydrological cycle of the Hadley Centre Climate model, HadCM3. This is a global non-flux-adjusted coupled atmosphere-ocean GCM. It has been shown to represent a stable and realistic oceanic and atmospheric circulation and climatology [*Gordon et al.*, 2000; *Sime et al.*, 2006] with an excellent match between modeled and observed estimates of poleward atmospheric and oceanic heat transport [*Cooper and Gordon*, 2002; *Dong and Sutton*, 2002]. This paper will describe the incorporation of the stable water isotopes ($H_2^{18}O$ and $HD^{16}O$, hereafter referred to as "isotopes") into the HadCM3 model and present preliminary results using $\delta^{18}O$ (where $\delta^{18}O$ is $\frac{(H_2^{18}O/H_2^{16}O)-VSMOW}{VSMOW} \times 1000$ and VSMOW is $H_2^{18}O/H_2^{16}O$ of Vienna Standard Mean Ocean Water). In particular we will focus on the isotopic signature of an El Niño event and the relationship between tropical precipitation and $\delta^{18}O$ of precipitation (hereafter referred to as $\delta^{18}O_p$).

[3] Present-day spatial correlations between $\delta^{18}O_p$ and climate variables show that $\delta^{18}O_p$ is most strongly correlated with temperature at high latitudes and most strongly correlated with precipitation amount in the tropics [*Dansgaard*, 1964]. The spatial relationship between precipitation amount and $\delta^{18}O_p$ (known as the spatial "amount effect") has been discussed by a number of modeling studies including *Mathieu et al.* [2002] and *Lee et al.* [2007]. However, these studies have correlated $\delta^{18}O_p$ with precipitation amount over the tropical oceans (20°N–20°S), and the regressions they find do not apply over the land where most paleoarchives of $\delta^{18}O_p$ occur. Here we consider the spatial amount effect in more detail to try and increase the understanding of how $\delta^{18}O_p$ is related to precipitation amount over the tropical ocean and land surface.

[1] Bristol Research Initiative for the Dynamic Global Environment, School of Geographical Sciences, University of Bristol, Bristol, UK.
[2] British Antarctic Survey, Cambridge, UK.

0148-0227/09/2008JD010825$09.00

[4] The El Niño Southern Oscillation (ENSO) is the single most important determinant of interannual variability in global precipitation fields [*Dai et al.*, 1997], yet it has not been fully investigated by other isotope enabled GCMs. Previous work, using isotope enabled atmospheric GCMs [*Hoffmann et al.*, 1998; *Noone and Simmonds*, 2002] found that the interannual, temporal correlation between precipitation and $\delta^{18}O_p$ reached a maximum over the central Pacific where the ENSO signal dominates, suggesting an ENSO imprint on $\delta^{18}O_p$. *Schmidt et al.* [2007] considered the isotopic signal of ENSO using the fully coupled GISS model and found the leading EOF of tropical SST variance to be correlated with $\delta^{18}O_p$ with regressions consistent with observations. A more complete investigation of ENSO was conducted by *Brown et al.* [2006], who coupled their isotope enabled AGCM to an interactive isotope ocean box model in order to investigate the imprint of El Niño on the $\delta^{18}O$ of sea water ($\delta^{18}O_{sw}$) and of corals. Correlations between the Southern Oscillation Index (SOI) and $\delta^{18}O_p$ were at a maximum over the central Pacific, and a similar correlation pattern was found between SOI and $\delta^{18}O_{sw}$. Their estimates of coral $\delta^{18}O$ were in reasonable agreement with observations at sites where precipitation was well simulated.

[5] HadCM3 includes water isotopes in a fully coupled system and has been shown to simulate ENSO as well as other current generation coupled models, with an amplitude and frequency that is broadly in agreement with observations [*Collins et al.*, 2001; *Latif et al.*, 2001; *AchutaRao and Sperber*, 2002]. The model is therefore in a unique position to investigate the isotopic signal of ENSO. Following *Brown et al.* [2006], we also consider the relationship of ENSO to $\delta^{18}O_p$, $\delta^{18}O_{sw}$ and $\delta^{18}O$ of corals, using the fully coupled model. In addition we use the climate anomaly associated with El Niño to investigate the spatial amount effect more fully and suggest ways in which the spatial correlation between precipitation amount and $\delta^{18}O_p$ can be increased.

[6] The new coupled atmosphere-ocean isotope model is described in section 2, and validated against present-day observations in section 3. Section 4 investigates the isotopic response to ENSO for the present-day climate, and section 5 considers the spatial amount effect. Results are summarized in section 6.

2. Model Description

[7] HadCM3 is a state of the art GCM that has been used in numerous scientific studies including the latest IPCC report. It is composed of two main components: an atmospheric component (HadAM3) and an oceanic component (HadOM3). These components can either be coupled together (as HadCM3) or run separately. Isotopes have been added to the full hydrological cycle of HadCM3 as described in the sections below. Here, it is worth noting that the different structure of HadAM3 and HadOM3 makes it necessary to use different techniques to incorporate isotopes into the two models. In particular, HadAM3 models water explicitly and so two new water species (to represent $H_2^{18}O$ and $HD^{16}O$) have been explicitly added to this model. In contrast, HadOM3, assumes a fixed volume of water in each model grid box which means that isotopes must be included as a tracer (in the same way as salinity) with each isotope species making up a fraction of each model grid box.

2.1. Atmospheric Model

[8] The atmospheric component of the Hadley Centre model (HadAM3) has been described by *Pope et al.* [2000]. It is a hydrostatic grid point model using an Arakawa B grid and hybrid vertical coordinates. The horizontal resolution is $3.75^\circ \times 2.5^\circ$, there are 19 vertical levels and 30 minutes time steps. The model uses a conservative split-explicit integration scheme with fourth-order horizontal advection as described by *Cullen and Davies* [1991]; such that the advection of water vapor and its isotopes depend upon their spatial gradients. Although this scheme leads to realistic results for both $H_2^{16}O$ and $H_2^{18}O$, it was able to cause some unrealistically large or small values of $\delta^{18}O_p$ because of small discrepancies between the gradients of the two water species. This problem is not unique to HadCM3 and has also occurred in other models, here it was overcome in the way suggested by *Mathieu et al.* [2002] for the GENESIS GCM, namely by redistributing isotopic mass to surrounding grid boxes when the advection scheme caused a large and physically unrealistic change in atmospheric $\delta^{18}O$.

2.1.1. Surface Evaporation

[9] In HadAM3, evaporation from the ocean surface is proportional to the difference between the saturated specific humidity at the surface and the specific humidity at the lowest atmospheric layer and includes both equilibrium and kinetic fractionation [*Merlivat and Jouzel*, 1979]. When calculating kinetic fractionation we use the diffusivities suggested by *Cappa et al.* [2003] which are more realistic. Sea ice is represented in the model and is either prescribed (HadAM3) or calculated by the oceanic component (HadCM3). Because of the slow diffusivity of heavy isotope species within ice, sublimation from sea ice is assumed to be nonfractionating.

[10] Many isotope enabled models use a "bucket" scheme to represent the land surface [e.g., *Mathieu et al.*, 2002; *Noone and Simmonds*, 2002] where precipitation minus evaporation minus runoff fills a shallow top layer while any overflow fills a lower layer of infinite capacity. These models make assumptions about the vegetation type at the surface and there is limited scope for interpreting isotopes within the surface hydrology. Recently, however, the GISS model has included water isotopes in a more sophisticated land surface scheme [*Aleinov and Schmidt*, 2006]. The introduction of isotopes into an advanced land surface scheme has been shown by *Fischer* [2006] to provide a new useful means of investigating and characterizing land surface behavior. Further, *Fischer* [2006] notes that the bucket schemes used in some models fail to reproduce the isotopic partitioning of a more complex land surface scheme. The land surface scheme used in HadCM3 is the MOSES2 land surface exchange scheme and includes the sophisticated TRIFFID dynamic vegetation model [*Cox et al.*, 1999]. MOSES2/TRIFFID uses several surface types (broadleaf trees, needleleaf trees, shrubs, C4 grass, C3 grass, bare soil, urban, water and snow/ice), which each make up a fraction of every grid box. There are 4 soil levels. Each surface type interacts with the climate and vegetation structure dynamically adjusts throughout a long model run. Precipitation will either be intercepted by the canopy, treated as runoff or

absorbed into the soil. Despite all these potential complexities, the isotopes are treated in a relatively simple way in the land surface scheme: there is no fractionation during evaporation from the vegetated land surface [*Zimmermann et al.*, 1967], during sublimation from ice (due to the slow diffusivities of $H_2^{18}O$ and $HD^{16}O$ in ice), or when exchanging water between adjacent soil layers. Although *Aleinov and Schmidt* [2006] suggested that evaporation from bare soil should fractionate, this fractionation is not currently included in HadCM3; however since evaporation from soil is typically only 10% of total evaporation its omission should have only a small impact on the overall results. Condensation as dew is considered to be non fractionating as this evaporates very rapidly, condensation onto snow includes kinetic fractionation analogous to that used when forming ice clouds as is described in the next section.

2.1.2. Condensation and Postcondensation Processes

[11] There are two condensation schemes in HadCM3, one which deals with large-scale nonconvective clouds and another which deals with convective clouds. The large-scale cloud scheme is based on *Smith* [1990] with modifications described by *Gregory and Morris* [1996]. This scheme contains prognostic variables for liquid water and ice clouds, and allows for mixed phase clouds when the temperature is between $-9°C$ and $0°C$. Clouds only form in those grid boxes which have relative humidity greater than a critical level of 70%. Liquid condensate is formed in isotopic equilibrium with the surrounding vapor, while the formation of frozen condensate includes a kinetic process due to the diffusion of isotopes around the oversaturated zone surrounding ice crystals. This kinetic process depends on a supersaturation function, Si, which is taken to be a linear function of temperature (T [*Jouzel and Merlivat*, 1984]). The parameterization of Si is not well constrained by data [*Jouzel*, 1986] and was originally taken to be $Si = 1-0.003T$ [*Jouzel et al.*, 1987], but more recently work [*Schmidt et al.*, 2005; *Lee et al.*, 2007] has increased the dependence of Si on temperature to $Si = 1 - 0.004T$. Here we use $Si = 1 - 0.005T$; the value of Si does not have a discernible effect on $\delta^{18}O_p$, but does allow for some tuning of the deuterium excess.

[12] Precipitation from stratiform clouds is assumed to form slowly and so it is assumed [*Hoffmann et al.*, 1998] that 95% of the precipitation reaches isotopic equilibrium with the vapor as it passes through lower layers. This means that the isotopic ratios at the lowest atmospheric levels (which are more strongly influenced by evaporation) will have the largest influence on the isotopic value of falling liquid precipitation. This is in agreement with the results of *Lee et al.* [2007] who quantified the importance of evaporation in determining $\delta^{18}O_p$ and showed that a Rayleigh distillation process alone was inadequate. Frozen condensate does not exchange with the surrounding vapor because of the low diffusivities of $H_2^{18}O$ and $HD^{16}O$ in ice. There is also no fractionation between $H_2^{18}O$ and $HD^{16}O$ on melting, freezing or sublimation [*Jouzel*, 1986].

[13] The convection scheme in HadCM3 is as described by *Gregory and Rowntree* [1990] but with the addition of convective downdrafts. Convective clouds form quickly and precipitate quickly meaning that they are not treated the same as large-scale clouds. Convective clouds are formed in isotopic equilibrium with surrounding vapor; the fractionation factors corresponding to the vapor-liquid phase transition is used for temperatures greater than $-20°C$ otherwise the vapor-solid phase transition is used. There has been some disagreement whether there should be a kinetic fractionation associated with the formation of convective ice clouds. For example the GENESIS model follows the suggestion of *Federer et al.* [1982] and does not include kinetic fractionation in the formation of ice clouds; however other isotope enabled GCMs follow *Jouzel and Merlivat* [1984] and include kinetic fractionation in the formation of ice clouds. Here we follow the methodology implemented in the majority of other GCMs and use kinetic fractionation, however we note that it will generally make little difference whether or not kinetic fractionation is included because of the effect of postcondensation processes and the fact that convective precipitation generally falls as liquid. As convective precipitation falls through lower layers there will be some exchange between condensate and vapor, however the precipitation falls more quickly and drops are larger than associated with large-scale precipitation and so the condensate does not have time to equilibrate fully with the surrounding vapor. Following *Hoffmann et al.* [1998] we assume that 45% of liquid convective precipitation reaches equilibrium with the surrounding air. Below the cloud base the air is unsaturated and any liquid precipitation will start to evaporate. Since this process can occur rapidly a kinetic isotope effect (described by *Stewart* [1975]) is required. This kinetic effect is proportional to $1 - h$, where h is the relative humidity, and so is more apparent at dry sites. *Jouzel et al.* [1987] noted that as raindrops evaporate the air will become gradually more saturated and so the influence of this kinetic effect decreases during the course of the precipitation event. For simplicity, and following *Jouzel et al.* [1987], the kinetic fractionation is calculated using a constant effective relative humidity h_{eff}, ($h_{eff} = 0.75 + 0.25h_i$; h_i is the initial relative humidity) which takes into account the changing relative humidity over the course of the precipitation event.

2.2. Ocean

[14] The oceanic component of HadCM3, HadOM3, is a standard "rigid lid" barotropic model. It is based on the GFDL "Cox" ocean model with modifications as described by *Gordon et al.* [2000]. The standard HadCM3 horizontal resolution is $1.25° \times 1.25°$, with 20 oceanic levels and 1 h time steps. HadCM3 does not require oceanic flux correction; however, since there is no representation of iceberg calving, a small prescribed water flux is returned to the ocean to balance the net accumulation of snowfall on the ice sheets. This water flux is converted to surface salinity fluxes using a constant reference salinity of 35 PSU.

[15] Since the HadCM3 ocean is represented by a rigid lid model the volume of the ocean is fixed and cannot be altered by water fluxes due to evaporation, precipitation or runoff. *Pardaens et al.* [2003] describe how water fluxes in HadCM3 are converted to a virtual salt flux such that the salinity of the top level of the ocean changes with freshwater inputs and the freshwater budget is conserved. The isotope budget is conserved in a similar way: water fluxes to the ocean (due to $H_2^{16}O$ in evaporation, precipitation and runoff) and isotope fluxes to the ocean (due to $H_2^{18}O$ in evaporation, precipitation and runoff) are converted to a virtual isotope

flux, analogous to the virtual salt flux. This virtual isotope flux alters the $H_2^{18}O/H_2^{16}O$ ratio in the top level of the ocean by an amount consistent with the water and isotope fluxes from the atmosphere and land surface.

[16] The isotopic tracers are mixed horizontally, using the version of the *Gent and McWilliams* [1990] scheme, which is incorporated into HadCM3. HadCM3 also comprises a simple sea ice model, this is based on the zero-layer model of *Semtner* [2006] and includes ice drifts, leads and snow cover. Ice is advected by the surface ocean current, with convergence prevented when the depth exceeds 4 m [*Cattle and Crossley*, 1995]. It has been shown to produce a realistic representation of ice extent by *Gregory et al.* [2002]. Ice processes are included in the new isotope scheme in the simplest possible way, since our first priority was the conservation of the isotope budgets. No fractionation is included when ice forms from ocean water, when ice melts, when the overlying snow melts or on sublimation. It is noted that a small fractionation should be included in sea ice formation for maximum accuracy [*Pfirman et al.*, 2004].

[17] Although HadCM3 does not require heat flux correction, a small water flux, which represents iceberg calving, is required to close the global hydrological cycle. Since iceberg calving also introduces $H_2^{18}O$ into the ocean a small isotope flux is also required. This isotope flux was prescribed with $\delta^{18}O = -30‰$ relative to the water flux, which is a reasonable estimate of $\delta^{18}O$ in high latitude sea ice. However since the isotope flux was not calculated directly from the model a very small drift in ocean isotopes remains. The drift is not large enough to affect the results of the century-scale simulations shown here and will be corrected at a later date.

[18] In order to allow a longer control run for analysis this paper uses HadCM3L: a version of HadCM3 with reduced oceanic horizontal resolution of $3.75° \times 2.5°$. The setup of HadCM3L is identical to that of HadCM3 except that the reduced ocean resolution requires a minor adjustment of the land-sea mask to maintain the present-day thermohaline circulation.

3. Validation: Present-Day Model-Data Comparison

[19] The isotope enabled version of HadAM3, has previously been considered by *Sime et al.* [2008] who showed that the geographical pattern of modeled present-day Antarctic $\delta^{18}O_p$ provided a good match with 20th century $\delta^{18}O$ Antarctic surface snow [*Masson-Delmotte et al.*, 2008]. Here we compare results from a 200 year preindustrial, HadCM3L control run with $\delta^{18}O$ from a number of sources, to assess the simulation of $\delta^{18}O$ both spatially and temporally. The control run was prescribed CO_2 of 280 ppmv and CH_4 of 760 ppbv. $\delta^{18}O$ was initialized to 0‰ over the ocean and in the land surface and −40‰ in snow and ice. The annual mean $\delta^{18}O_p$ from the model is compared with observations in Figure 1, where Figure 1a shows $\delta^{18}O_p$ averaged over the last 10 years of the control simulation and Figure 1b shows $\delta^{18}O_p$ provided by the Global Network of Isotopes in Precipitation (GNIP) observational database. The GNIP data is limited to those stations which contain a full annual cycle of observations, further information about GNIP can be found at

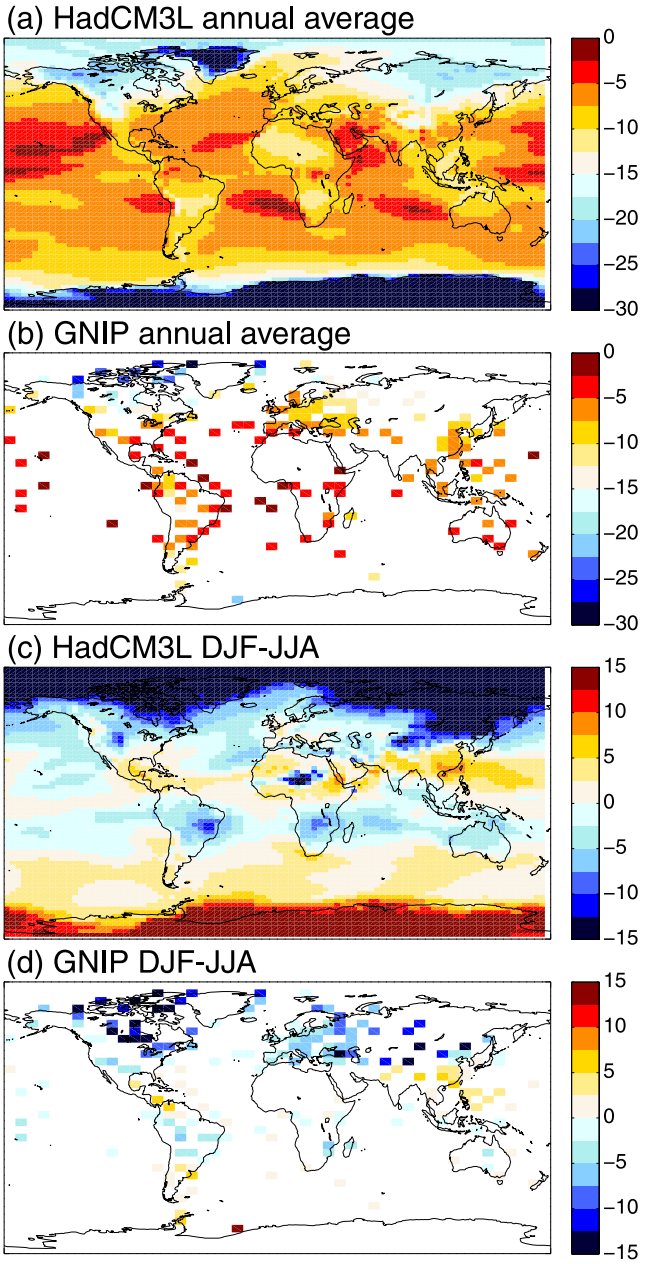

Figure 1. Comparison between HadCM3L and GNIP. (a and b) Long-term annual average $\delta^{18}O_p$ and (c and d) long-term seasonality (DJF-JJA) of $\delta^{18}O_p$.

http://www-naweb.iaea.org/napc/ih/GNIP/HIS_GNIP.html. The modeled results compare well with GNIP over most of the globe, although the scarcity of the observations makes a full comparison difficult. The four standard determinants of $\delta^{18}O_p$ are clearly visible in Figure 1a: the amount effect over the tropical oceans with $\delta^{18}O_p$ more depleted over wetter regions, the temperature effect at higher latitudes with $\delta^{18}O_p$ more depleted over the colder regions, the continentality effect with $\delta^{18}O_p$ more depleted further from its ocean source and the altitude effect with $\delta^{18}O_p$ more depleted at higher altitudes. These features have been seen in other models and are described in detail by *Mathieu et al.* [2002].

[20] Although overall the isotope model compares well with observations, the modeled $\delta^{18}O_p$ over tropical continents is

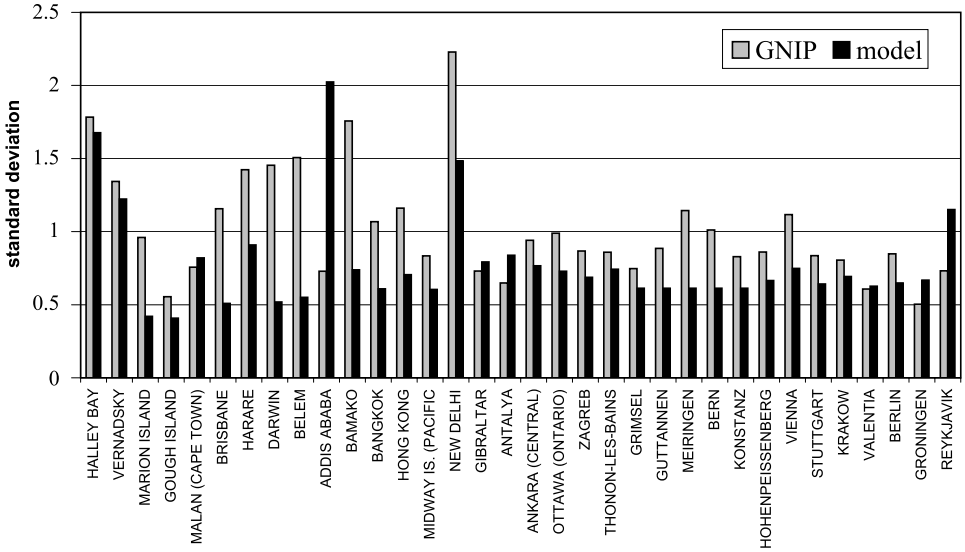

Figure 2. Interannual standard deviation of $\delta^{18}O_p$ from HadCM3 (black) and GNIP (light gray). Coordinates for the stations are Halley Bay (76°S, 21°W), Vernadsky (65°S, 64°W), Marion Island (47°S, 39°E), Gough Island (40°S, 10°W), Malan (34°S, 19°W), Brisbane (27°S, 153°E), Harare (18°S, 31°E), Darwin (12°S, 131°E), Belem (1°S, 48°W), Addis Ababa (9°N, 39°E), Bamako (12°N, 8°W), Bangkok (14°N, 100°E), Hong Kong (22°N, 114°E), Midway Island (28°N, 177°W), New Delhi (23°N, 77°E), Gibraltar (36°N, 5°W), Antalya (37°N, 31°E), Ankara (40°N, 33°E), Ottawa (45°N, 76°W), Zagreb (46°N, 16°E), Thonon-Les-Bains (46°N, 6°E), Grimsel (47°N, 8°E), Guttannen (47°N, 8°E), Meiringen (47°N, 8°E), Bern (47°N, 8°E), Konstanz (48°N, 9°E), Hohenpeissenberg (48°N, 11°E), Vienna (48°N, 16°E), Stuttgart (49°N, 9°E), Krakow (50°N, 20°E), Valentia (52°N, 10°W), Berlin (53°N, 13°E), Groningen (53°N, 6°E), and Reykjavik (64°N, 22°W).

generally too depleted. *Hoffmann et al.* [1998] suggested including a global enrichment of the ocean surface of 0.5‰ when calculating the evaporation from the ocean; this enrichment was included in an early version of our model and initially resulted in greater agreement between tropical $\delta^{18}O_p$ from the model and tropical $\delta^{18}O_p$ from GNIP (although the global enrichment alone was not sufficient to explain the full discrepancy over the tropical continents). However, this isotopic enrichment led to an additional export of $H_2^{18}O$ from, and thus more depleted $H_2^{18}O$ remaining in, those regions with high evaporation. Over the longer term this led to a large mismatch between modeled $\delta^{18}O_{sw}$ and observed $\delta^{18}O_{sw}$, a consequence which would not be apparent in an atmosphere only model such as that used by *Hoffmann et al.* [1998]. The global enrichment has not been included in the current version of HadCM3 and hence the tropical values of $\delta^{18}O_p$ are more depleted than they would otherwise have been. The tropical continental $\delta^{18}O_p$ is also too depleted in the NCAR model [*Lee et al.*, 2007], where it has been attributed to inaccuracies in the modeled climate. The HadCM3 climate is in reasonable agreement with observations [e.g., *Johns et al.*, 2003], and there is no systematic precipitation bias between HadCM3L and GNIP over the tropics (not shown). This suggests it is unlikely that the negative $\delta^{18}O_p$ bias in HadCM3 can be fully explained by inaccuracies in the modeled climate. Since the discrepancies are larger over land there may be some issues with the hydrology or the treatment of isotopes within the land surface scheme.

[21] Figures 1c and 1d show the long-term mean seasonality (DJF-JJA) of $\delta^{18}O_p$, for HadCM3L and the GNIP observations respectively. Again a scarcity of data points makes a full comparison difficult; however there appears to be very good agreement between the model and the data everywhere, even over the tropical continents where the modeled annual average $\delta^{18}O_p$ was too depleted. It has been argued that the relationship between $\delta^{18}O_p$ and climate over the seasonal cycle might be useful for paleoclimatic applications because different climate forcings occur at different times of the year [*Siegenthaler and Oeschger*, 1980]. If this is the case than the good agreement between model and data seasonal cycles in Figure 1 supports the use of the model for paleoclimate applications throughout the globe. However, *Rozanski et al.* [1992] suggested that the interannual relationship between $\delta^{18}O_p$ and climate parameters would be more appropriate for paleoclimatic reconstructions.

[22] Many GNIP stations provide isotopic measurements from a small number of years, and so provide little information about the interannual variability of $\delta^{18}O_p$. The following analysis is therefore limited to those GNIP stations which contain more than 20 years of data. To investigate the interannual variability of $\delta^{18}O_p$ in the model the interannual standard deviation was calculated from precipitation weighted annual $\delta^{18}O_p$ for each GNIP station and the corresponding model grid box. This is shown in Figure 2. Generally the standard deviation from GNIP is larger than that calculated by the model. This is reasonable since GNIP stations represent $\delta^{18}O_p$ over a spatially small sample site while the model represents $\delta^{18}O_p$ over a large grid box. The modeled variability is similar to the GNIP variability at mid and high latitudes where $\delta^{18}O_p$ is related to temperature, while the modeled variability is much smaller than the GNIP variability

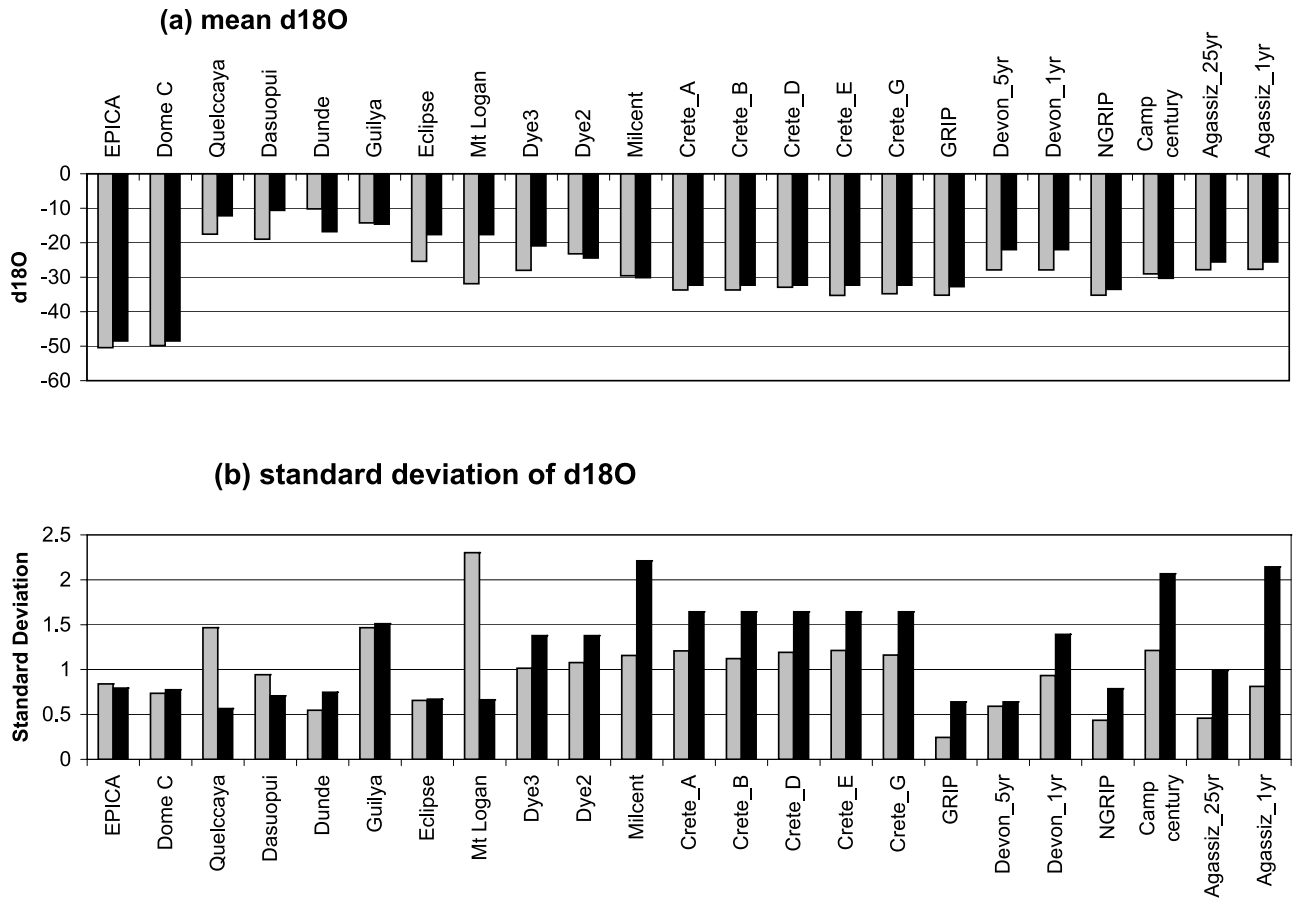

Figure 3. A comparison between the modeled $\delta^{18}O_p$ and ice core data. In each case the gray bar shows results from the ice core while the black bar shows the results from the model. The temporal resolution of each ice core record and its coordinates are as follows: EPICA, 9 years (75°S, 123°E); Dome C, 11 years (74°S, 123°E); Quelccaya, 1 year (14°S, 71°W); Dasuopui, 10 years (28°N, 85°E); Dunde, 10 years (38°N, 96°E); Guilya, 10 years (39°N, 81°E); Eclipse, 1 year (61°N, 139°W); Mount Logan, 1 year (61°N, 140°W); Dye3, 1 year (65°N, 43°W); Dye2, 1 year (66°N, 46°W); Milcent, 1 year (70°N, 44°W); Crete, 1 year (71°N, 37°W); GRIP, 20 years (72°N, 37°W); Devon, 5 years and 1 year (75°N, 89°W); NGRIP, 20 years (76°N, 42°W); Camp Century, 1 year (77°N, 61°W); and Agassiz, 25 years and 1 year (81°N, 73°W).

over the tropics where $\delta^{18}O_p$ is related to precipitation amount. Perhaps this is because precipitation is spatially more noisy than temperature, and so spatial smoothing of precipitation over a large model grid box would reduce the modeled variability of $\delta^{18}O_p$ relative to the data in those regions where $\delta^{18}O_p$ is related to precipitation amount.

[23] Although the present-day interannual comparison with GNIP is important, it is also important to compare isotope information from the model to longer-term data, such as that provided by ice cores. Here we briefly compare $\delta^{18}O_p$ from the 200 year HadCM3 control simulation to the last 200 years of ice core data obtained from various stations around the globe. The ice core data used is publicly available at the National Climatic Data Center.

[24] Figure 3 compares model results and ice core data for the mean $\delta^{18}O$ and interannual standard deviation of $\delta^{18}O$. In each case the light gray bar represents the ice core data while the black bar represents the model data. There is good agreement between mean $\delta^{18}O$ from the data and the model, however, where a discrepancy does exist it is nearly always the data that is more depleted. The largest discrepancy occurs over Mount Logan (61°N, 140°W)where the data is −14‰ more depleted than the model. This is probably due to the "altitude effect" as Mount Logan is not large enough to cover a whole model grid box and so while the data was taken from a point 5340 m high the model grid box altitude is only 1080 m. Mount Logan is also the ice core which has the largest discrepancy between model and data in standard deviation, again this could be due to the model being unable to accurately resolve small-scale orography.

[25] The model and ice cores are reasonably consistent in standard deviation; however the Greenland sites generally have higher standard deviation in the model while the tropical sites generally have higher standard deviation in the ice cores. Assuming both model and data are accurate, differences between the two are likely to represent the effects of comparing a large model grid box to a site point and of larger postdeposition isotope diffusion in the high latitude lower accumulation rate ice cores. These factors have opposing influences; the differences in scale (which would

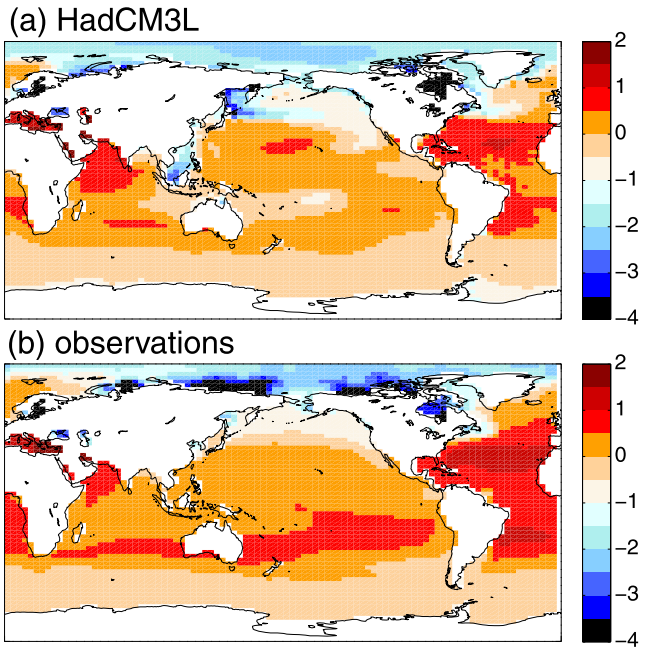

Figure 4. Mean $\delta^{18}O_{sw}$ for the top 50 m of the ocean surface: (a) an average of the last 10 years of the 200 year HadCM3L control simulation and (b) *Legrande and Schmidt* [2006] gridded data set based on observations.

be more important in the tropics where precipitation is related to $\delta^{18}O_p$) would reduce the model standard deviation relative to the ice cores while the postdepositional and codepositional processes (which would be more important over Greenland where surface winds are larger and the accumulation rate is lower) would reduce the ice core standard deviation relative to the model. Together these factors can explain at least some of the discrepancies between the model and ice core standard deviation. It is also noted that there are some important areas of agreement in the standard deviation of model and ice cores: the relative size of standard deviation between different Greenland sites is consistent between model and ice cores and there is remarkable agreement between model and data over Antarctica.

[26] Since HadCM3, is a coupled ocean-atmosphere GCM it is appropriate to consider the mean isotopic signal at the ocean surface. Figure 4 shows the $\delta^{18}O_{sw}$, averaged over the top 50 m of the ocean from the last 10 years of the HadCM3L control simulation (Figure 4a) and the *LeGrande and Schmidt* [2006] gridded data set based on observations (Figure 4b). It can be seen that the modeled values are very similar to the gridded observations over most of the globe, however there are some discrepancies. Over some regions of the tropics modeled $\delta^{18}O_{sw}$ is too depleted, this is particularly apparent near Australia, and is likely due to the fact that $\delta^{18}O_p$ is too depleted in these regions (see Figure 1). In addition the model is more depleted than the gridded observations over some coastal regions, particularly eastern Asia and North Eastern Canada. The depleted modeled $\delta^{18}O_{sw}$ in coastal regions is a result of the continental runoff of $\delta^{18}O_p$ mixing with the ocean waters. Further development and tuning of the runoff scheme may improve the representation of isotopes in $\delta^{18}O_{sw}$ although this is beyond the scope of this study.

[27] This section has shown that the isotopic scheme in HadCM3 is reasonable when compared with much of the data available, for both $\delta^{18}O_p$ and $\delta^{18}O_{sw}$. This gives confidence in our use of the isotope model to investigate the El Niño–Southern Oscillation (ENSO) coupled ocean-atmosphere climate phenomenon, which will allow further assessment of the isotope model. In addition, the reconstruction of modes of climate variability (such as ENSO) is often a goal of paleoclimate reconstructions, these reconstructions would be aided by model simulations of isotope responses to large-scale climate variability.

4. ENSO, $\delta^{18}O$, and the Tropical Amount Effect

[28] El Niño events were identified in the model simulation using the definition of *Trenberth* [1997] for the NINO3 region (90–150°W and 5°N–5°S). First, monthly mean SST's anomalies were calculated and a 5 month running mean applied. Anomalies, in the resulting time series, greater than 0.5°C for more than 6 months were categorized as "El Niño," while anomalies less than −0.5°C for more than 6 months were categorized as "La Niña." The NINO3 region was used instead of the NINO3.4 region as this is the location of the largest interannual SST variability in the standard HadCM3 model [*Brown et al.*, 2008]; although sensitivity tests (not shown) indicate that using the NINO3.4 region does not give significantly different results. El Niño and La Niña states of the model were than combined into El Niño and La Niña composites. The composites represented annual average conditions and so each El Niño month in the control simulation was weighted by the likelihood of an El Niño in that calendar month to account for the fact that El Niño is more prevalent in the NH winter.

[29] Figure 5 shows the El Niño composite anomaly relative to the long-term mean climate. Generally the La Niña anomalies are the inverse of El Niño anomalies, and so the discussion that follows will describe the El Niño anomalies only. Figure 5a shows the warm surface temperature anomaly, in the central Pacific and along the western coast of South America, which characterizes the El Niño state of the climate. Precipitation anomalies associated with El Niño are shown in Figure 5b. It can be seen that there is increased precipitation associated with El Niño across the full breadth of the Pacific Ocean. For the most part, the precipitation anomalies compare well with observations [*Dai and Wigley*, 2000; *Spencer and Slingo*, 2003], however the model fails to simulate the dry conditions of El Niño that occur in the western Pacific warm pool. This could be due to the fact that the *Gregory and Rowntree* [1990] convection scheme is closed on the buoyancy of the near surface air, causing regions of largest precipitation anomalies to occur over the regions of largest SST anomalies [*Spencer and Slingo*, 2003].

[30] Figure 5c shows the $\delta^{18}O_p$ anomaly for El Niño. As expected, this is clearly related to the precipitation anomaly, with depleted $\delta^{18}O_p$ over areas of increased precipitation and enriched $\delta^{18}O_p$ over areas of decreased precipitation. The $\delta^{18}O_p$ signal is much noisier than the precipitation signal, partly because Figure 5b is dominated by "wet" regions which have greatest potential for a large precipitation

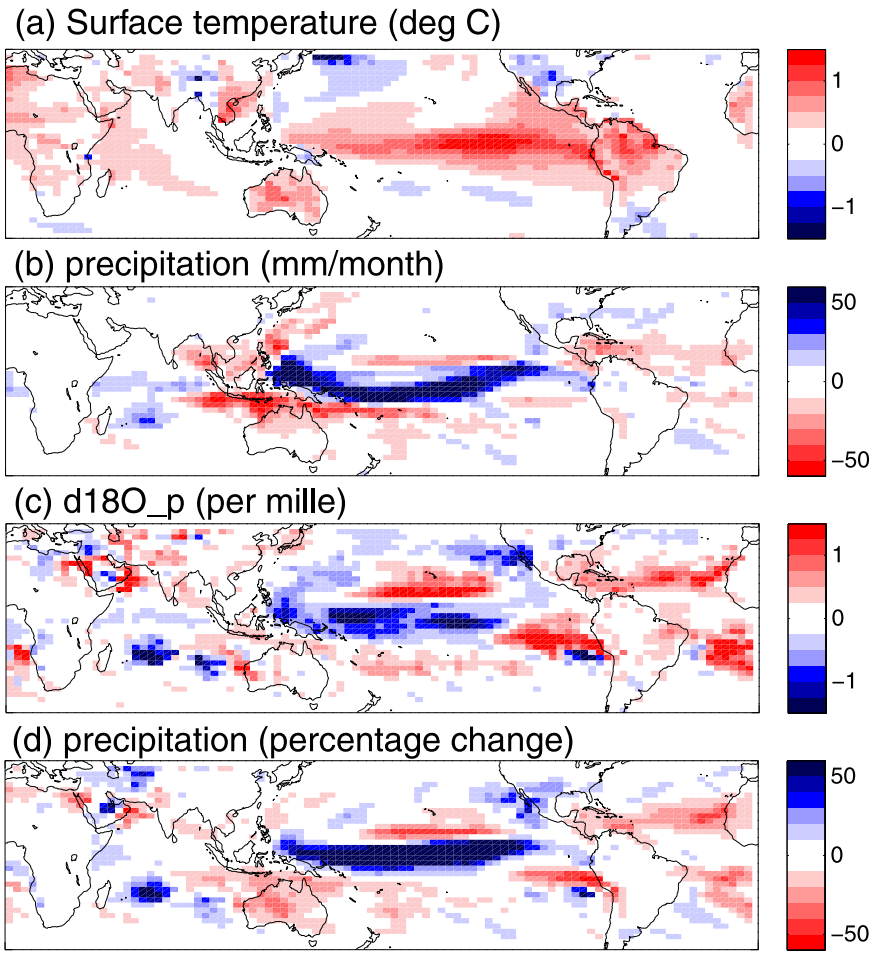

Figure 5. HadCM3L difference between El Niño composite and the long-term mean climate.

change (in mm/month). A weighted precipitation anomaly (Figure 5d) is therefore also included, which shows the percentage change in rainfall between the composite El Niño and the long-term mean. More precipitation anomalies are visible when the anomalies are weighted and there are some improvements in the correlation between $\delta^{18}O_p$ and precipitation amount (e.g., South Atlantic). A comparison between Figures 5c and 5d suggests that most tropical $\delta^{18}O_p$ anomalies are related to precipitation anomalies; although there is sometimes a spatial shift between the two variables consistent with the effects of the upstream rainout on $\delta^{18}O_p$. Given the clear relationship between $\delta^{18}O_p$ and precipitation, it follows any errors in precipitation associated with El Niño, will likely propagate to errors in $\delta^{18}O_p$.

[31] Figure 6a shows the $\delta^{18}O_{sw}$ anomaly associated with El Niño. As expected the oceanic effect is largest in coastal regions, where the shallow mixed layer depth, and increased mixing due to surface runoff, allow interannual changes in precipitation to be seen in the ocean. In contrast, *Brown et al.* [2006] found the largest El Niño $\delta^{18}O_{sw}$ signal in the central Pacific, however their rather simple model did not include runoff. The El Niño, $\delta^{18}O_{sw}$ anomaly is particularly pronounced in the Southwest Pacific; this was discussed by *Tudhope et al.* [1995] who found enriched $\delta^{18}O_{sw}$ associated with El Niño in this region. Unfortunately the model fails to reproduce the reduced precipitation and enriched $\delta^{18}O_p$ in this region, and hence the $\delta^{18}O_{sw}$ signal, whilst being consistent with the model physics and of a similar magnitude to observations, is not of the same sign.

[32] The modeled SST and $\delta^{18}O_{sw}$ El Niño anomalies were combined to estimate the $\delta^{18}O$ El Niño anomaly that

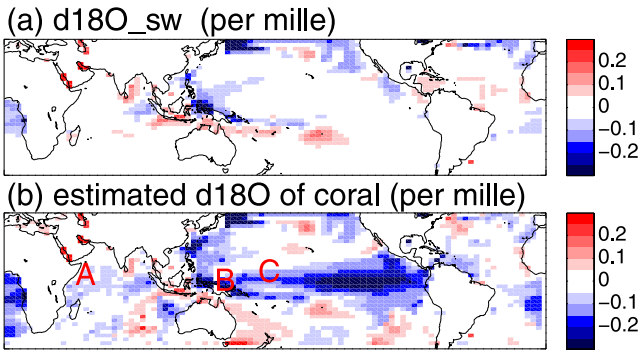

Figure 6. HadCM3L difference between the El Niño composite and the long-term mean climate: (a) $\delta^{18}O_{sw}$ for the top 10 m of the ocean and (b) $\delta^{18}O$ of coral estimated using the model results and the empirical equation of *Juillet-Leclerc and Schmidt* [2001]. The red letters denote the locations of the observational sites at Mahe Island (site A), Madang (site B), and Maiana Island (site C) that are discussed in the text.

Table 1. Comparison of Modeled Coral $\delta^{18}O$ and Observed Coral $\delta^{18}O$ at Three Sites[a]

Site	Location	EN-LTM Model (Data)	EN-LN Model (Data)	Years of Data
Site A: Mahe Island	4°S, 55°E	−0.06 (−0.04)	−0.10 (−0.09)	1950–1994
Site B: Madang	5°S, 145°E	−0.27 (0.16)	−0.39 (0.23)	1950–1990
Site C: Maiana Island	1°N, 173°E	−0.13 (−0.20)	−0.25 (−0.36)	1950–1994

[a]Observed values are in brackets. EN-LTM is the difference between the El Niño composite and the long-term mean climate, and EN-LN is the difference between the El Niño composite and the La Niña composite.

would be seen in coral data. This was done using the empirical relationship derived by *Juillet-Leclerc and Schmidt* [2001]: $\delta^{18}O_{coral} = \delta^{18}O_{sw} + (0.2 \times SST) + 0.45$ and is shown in Figure 6b. The empirical relationship was developed using Porites coral from a large number of colonies collected from different sites over the temperature range 24°–30°C. Figure 6b shows that $\delta^{18}O$ of coral is related to SST over most of the ocean and to $\delta^{18}O_{sw}$ in coastal regions. Highlighted in Figure 6b are three coral sites, data from which will be compared with the modeled results. The sites are: Maha Island in the Indian Ocean (site A [*Charles et al.*, 1997]), Madang in the Western Pacific (site B [*Tudhope et al.*, 2001]) and Maiana Island in the Central Pacific (site C [*Urban et al.*, 2000]). These sites have previously been compared with an isotope model by *Brown et al.* [2006].

[33] Table 1 compares modeled coral $\delta^{18}O$ and observed coral $\delta^{18}O$ for the three sites. The comparison is made for El Niño anomalies relative to both the long-term mean and the La Niña composite. The observed El Niño and La Niña were obtained, on the basis of the NINO3 index, in the same way as calculated for the model. It can be seen that the modeled $\delta^{18}O$ coral anomaly is similar to the observed anomaly at both Mahe Island (Indian Ocean) and Maiana Island (Central Pacific), especially when we note that the modeled results are not intended to represent any particular calendar years and that the observed results will contain El Niño and La Niña events of a different magnitude to those in the model. The modeled coral $\delta^{18}O$ anomalies at Madang are not in good agreement with observations, again because of the error in simulating El Niño precipitation over the Western Pacific.

[34] Despite the poor agreement between model and data at Madang, it is still useful to assess the relative importance of SST and $\delta^{18}O_{sw}$ to coral $\delta^{18}O$ in this region. The model suggests that SST changes contribute only about one third of the coral $\delta^{18}O$ anomalies at Madang; this means that the model results agree with *Tudhope et al.* [1995] in the sense that the coral anomalies due to El Niño are predominantly an indication of $\delta^{18}O_{sw}$ in this region. In contrast, at Mahe and Maiana, $\delta^{18}O_{sw}$ typically contributes about 10% of the coral $\delta^{18}O$, implying that the ENSO signal here reflects changes in SST; in agreement with observations at Mahe Island [*Charles et al.*, 1997].

5. Spatial "Amount Effect"

[35] One feature that is typical of isotope enabled GCMs is that the correlation between precipitation amount and $\delta^{18}O_p$ is larger in the models than in the observations; this appears to be the case for spatial correlations [e.g., *Lee et al.*, 2007; *Mathieu et al.*, 2002] and for interannual temporal correlations [*Cole et al.*, 1999; *Hoffmann et al.*, 1998]. Although this discrepancy could be due to a systematic error there is the possibility that both the model and the data are correct. Observations over the Andean region [*Hoffmann et al.*, 2003] and model results [*Schmidt et al.*, 2007] suggest that $\delta^{18}O_p$ provides a record of large-scale regional precipitation rather than local precipitation. If indeed this is the case then $\delta^{18}O_p$ would be more strongly correlated with precipitation over a large model grid box than with precipitation at a small observation site. It is therefore appropriate to consider the modeled amount effect in more detail.

[36] *Mathieu et al.* [2002] considered the spatial amount effect over the tropical oceans (20°N–20°S) for a 3 year run of their GCM. They found the least squares regression slope between $\delta^{18}O_p$ and precipitation to be −1.14‰/(mm/a), and noted that this was not significantly different from observations. The least squares regression slope from HadCM3 is also −1.14‰/(mm/a) and has $r^2 = 0.56$. The correlation between $\delta^{18}O_p$ and precipitation amount over the tropical oceans is interesting theoretically but has limited practical applications for oceanic paleoproxies. Oceanic paleoproxies, such as corals, will provide information about $\delta^{18}O_{sw}$ and SST and cannot be translated to precipitation amount using this relationship. Paleoproxies over the land (such as tree rings and ice cores) can provide information about precipitation amount, however precipitation amount and $\delta^{18}O_p$ are less correlated over land; for example including tropical land points into the regression from HadCM3 reduces r^2 from 0.56 to 0.30.

[37] It will now be considered whether there is a more robust spatial correlation between tropical $\delta^{18}O_p$ and tropical precipitation amount when both can be attributed to a consistent source (e.g., an El Niño event) instead of when the two variables are obtained from climatological means. Figure 5 suggests that the El Niño precipitation anomaly is related to the El Niño $\delta^{18}O_p$ anomaly and that the relationship is stronger when the precipitation difference is expressed as a percentage change rather than in mm/month. This is confirmed quantitatively in Figure 7 which shows r^2 calculated from precipitation anomalies and $\delta^{18}O_p$ anomalies for different latitude bands of the globe. r^2 values have been obtained using precipitation changes expressed both as a percentage and in mm/month for the El Niño minus the long-term mean climate, the La Niña minus the long-term mean climate and the El Niño minus the La Niña climate. Figure 7 shows that for all latitude bands and for all climate anomalies, precipitation and $\delta^{18}O_p$ are much stronger correlated when precipitation change is expressed as a percentage. This improvement is substantial, for example within the latitudes 20°N–20°S, approximately twice the precipitation variability can be explained by $\delta^{18}O_p$ variability when precipitation change is expressed as a percentage and large improvements are also seen in other latitude bands.

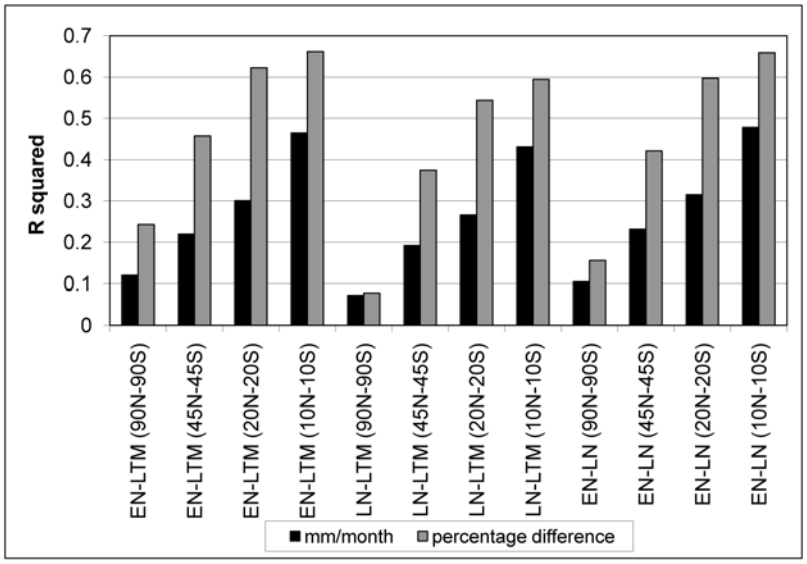

Figure 7. Relationship between precipitation anomalies and $\delta^{18}O_p$ anomalies for different latitude bands of the globe. (EN, El Niño composite; LTM, long-term mean climate; and LN, La Niña composite.)

[38] Figure 8 shows the spatial relationship between precipitation amount and $\delta^{18}O_p$ and how this differs between ocean grid boxes (black crosses) and land grid boxes (red crosses). While the spatial variability in the El Niño anomalies (Figures 8a and 8b) is dominated by ocean points the land points appear consistent with the ocean regressions. Though we note that when the mm/month change in precipitation is used (Figure 8b) the simple linear spatial relationship between precipitation and $\delta^{18}O_p$ breaks down both over the land and the ocean. Figure 8c shows however, that when considering annual average values, the spatial relationship between precipitation amount and $\delta^{18}O_p$ is inconsistent between the land and the ocean grid cells. This is probably why some previous studies which have given regression results for the spatial precipitation amount effect [e.g., *Mathieu et al.*, 2002] have limited their analysis to oceanic grid boxes only.

[39] Figure 8 suggests that there is a simple spatial relationship between $\delta^{18}O_p$ anomalies and precipitation anomalies over land points for the El Niño composite relative to the long-term mean. For land points, if precipitation anomalies are expressed as a percentage change then $r^2 = 0.29$ for 10°N–10°S and $r^2 = 0.24$ for 20°N–20°S. If precipitation anomalies are expressed in mm/month r^2 is similar (0.30) over 10°N–10°S but is greatly reduced (0.13) over 20°N–20°S. This shows that, for land points, it is important to express precipitation anomalies as percentage changes away from the deepest tropics. For the 45°N–45°S and global regions there is no clear correlation between the precipitation anomalies and $\delta^{18}O_p$ anomalies over land points ($r^2 < 0.05$) regardless of how the precipitation anomalies are obtained.

[40] The standard spatial ''amount effect'' has often been calculated only with respect to the tropical oceans [e.g., *Mathieu et al.*, 2002]; it is here suggested that the amount effect over land points is consistent with the amount effect over ocean points if climate anomalies (e.g., El Niño, long-term mean) are used. We note however that for the region 20°N–20°S, r^2 over the land surface (≈0.3) is much less than that over the full region (≈0.65). This difference may not necessarily mean that the regressions are less appropriate over the land but rather that the El Niño signal is much stronger over the ocean and so the signal to noise ratio (both in precipitation and $\delta^{18}O_p$) is stronger over the ocean.

6. Discussion and Conclusions

[41] The addition of stable water isotopes to both the atmospheric and oceanic components of HadCM3 has been described. Modeled $\delta^{18}O$ for the modern climate compares well with data from a number of sources (such as GNIP, corals and ice cores) and on different time scales (annually, seasonally and interannually). While there are some discrepancies between the model and data many of these discrepancies can be related to either changes in scale between the model grid box and the data site, or the model being unable to fully resolve orography. Other discrepancies may represent more general problems with the modeled climate; for example the model does not accurately simulate the precipitation anomaly associated with El Niño over the Western Pacific and hence cannot be expected to accurately simulate the corresponding $\delta^{18}O_p$ anomaly. The largest discrepancy between model and data occurs over the tropical continents in annual mean $\delta^{18}O_p$ and requires further investigation, although this discrepancy is not confined to the HadCM3 model [*Lee et al.*, 2007].

[42] Our investigation of the isotopic anomaly associated with the present-day ENSO shows that the $\delta^{18}O_p$ anomaly is correlated with the precipitation anomaly. The $\delta^{18}O_{sw}$ anomaly is also related to the precipitation anomaly but is strongest in coastal regions because of the influence of runoff. Estimating the coral $\delta^{18}O$ anomaly as a combination of $\delta^{18}O_{sw}$ and sea surface temperature shows the former is more important in coastal regions where there is a large $\delta^{18}O_{sw}$ signal. One region of model error, namely increased precipitation over the Western Pacific in El Niño years,

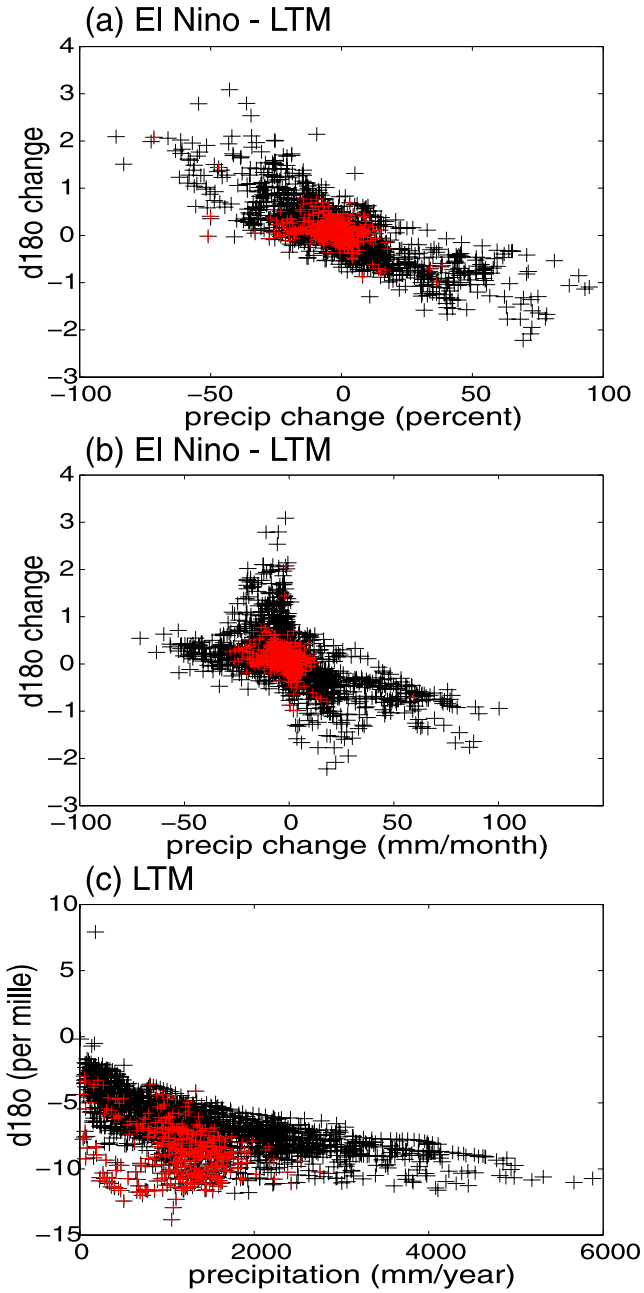

Figure 8. Spatial relationship between precipitation amount and $\delta^{18}O_p$ for the region 20°N–20°S. Black crosses are ocean points, and red crosses are land points. (a and b) Anomalies between El Niño and the long-term mean climate, with precipitation change measured as a percentage (Figure 8a) and in mm/month (Figure 8b). (c) The long-term mean annual average values of precipitation and $\delta^{18}O_p$.

propagates through to the isotopic model results and leads to errors in the modeled $\delta^{18}O_{sw}$ and estimated coral $\delta^{18}O$ in this region. In regions where the modeled precipitation and sea surface temperatures are reasonable there is good agreement between estimated and observed coral $\delta^{18}O$ changes associated with El Niño.

[43] The spatial correlation between $\delta^{18}O_p$ and precipitation amount is stronger when using the El Niño anomalies instead of annual mean precipitation and annual mean $\delta^{18}O_p$. The correlation is improved further when precipitation anomalies are weighted by precipitation amount and presented in units of percentage change. This improvement is particularly apparent over land points where the spatial amount effect was originally considered weak, and in the regions 10–20°N and 10–20°S. It is suggested that the improved correlation between $\delta^{18}O_p$ and precipitation amount will help with the interpretation of paleodata, and, although a full analysis of this is beyond the scope of this paper, some discussion is desirable.

[44] The weighted spatial correlation can be used to more accurately understand paleoclimatic anomalies (particularly those associated with El Niño) and investigate how the precipitation patterns of such anomalies have changed over time. They could also be used to suggest changes in circulation patterns for different periods. Although we note that many observations throughout the tropics would be required to calculate such spatial correlations which may prove a heavy observational requirement. In addition, when using the spatial correlation calculated using precipitation anomalies expressed as a percentage change, prior knowledge about the precipitation distribution over the tropics is required to reproduce precipitation anomalies (in mm/month) although this prior knowledge would not be required if it were sufficient to just know percentage precipitation changes at different locations.

[45] We have shown that the newly isotope enabled version of HadCM3 is a useful tool to investigate both isotopic climate anomalies and the relationship between $\delta^{18}O$ and climate parameters. Thus it will aid in our understanding of past climate systems. The analysis presented here should help in the interpretation of $\delta^{18}O$ in the tropical regions.

[46] **Acknowledgments.** This work was funded by NERC, under the RAPID thematic program. We would like to thank two anonymous reviewers for providing useful and insightful comments on a previous version of this manuscript.

References

AchutaRao, K., and K. Sperber (2002), Simulation of the El Nino Southern Oscillation: Results from the Coupled Model Intercomparison Project, *Clim. Dyn.*, *19*, 191–209.

Aleinov, I., and G. Schmidt (2006), Water isotopes in the GISS ModelE land surface scheme, *Global Planet. Change*, *51*(1–2), 108–120.

Brown, J., I. Simmonds, and D. Noone (2006), Modeling $\delta^{18}O$ in tropical precipitation and the surface ocean for present-day climate, *J. Geophys. Res.*, *111*, D05105, doi:10.1029/2004JD005611.

Brown, J., M. Collins, A. Tudhope, and T. Toniazzo (2008), Modelling mid-Holocene tropical climate and ENSO variability: Towards constraining predictions of future change with palaeo-data, *Clim. Dyn.*, *30*, 19–36.

Cappa, C. D., M. B. Hendricks, D. J. DePaolo, and R. C. Cohen (2003), Isotopic fractionation of water during evaporation, *J. Geophys. Res.*, *108*(D16), 4525, doi:10.1029/2003JD003597.

Cattle, H., and J. Crossley (1995), Modeling arctic climate change, *Philos. Trans. R. Soc. London, Ser. A*, *352*(1699), 201–213.

Charles, C., D. Hunter, and R. G. Fairbanks (1997), Interaction between the ENSO and the Asian monsoon in a coral record of tropical climate, *Science*, *277*(5328), 925–928.

Cole, J., D. Rind, R. Webb, J. Jouzel, R. Healy, C. Cooper, and C. Gordon (1999), Climatic controls on interannual variability of precipitation $\delta^{18}O$: Simulated influence of temperature, precipitation amount, and vapor source region, *J. Geophys. Res.*, *104*(D12), 14,223–14,235.

Collins, M., S. Tett, and C. Cooper (2001), The internal climate variability of HadCM3, a version of the Hadley Centre coupled model without flux adjustments, *Clim. Dyn.*, *17*, 61–81.

Cooper, C., and C. Gordon (2002), North Atlantic oceanic decadal variability in the Hadley Centre coupled model, *J. Clim.*, *15*, 45–72.

Cox, P., R. Betts, C. Bunton, R. Essery, P. Rowntree, and J. Smith (1999), The impact of new land surface physics on the GCM simulation of climate and climate sensitivity, *Clim. Dyn.*, *15*(3), 183–203.

Cullen, M., and T. Davies (1991), A conservative split-explicit integration scheme with 4th-order horizonal advection, *Q. J. R. Meteorol. Soc.*, *117*(501), 993–1002.

Dai, A., and T. Wigley (2000), Global patterns of ENSO-induced precipitation, *Geophys. Res. Lett.*, *27*, 1283–1286.

Dai, A., I. Fung, and A. DelGenio (1997), Surface observed global land precipitation variations during 1900–88, *J. Clim.*, *10*, 2943–2962.

Dansgaard, W. (1964), Stable isotopes in precipitation, *Tellus*, *16*, 436–468.

Dansgaard, W., et al. (1993), Evidence for general instability of past climate from a 250-kyr ice-core record, *Nature*, *364*(6434), 218–220.

Dong, B. W., and R. T. Sutton (2002), Variability in North Atlantic heat content and heat transport in a coupled ocean-atmosphere GCM, *Clim. Dyn.*, *19*, 485–497.

Federer, B., N. Brichet, and J. Jouzel (1982), Stable isotopes in hailstones. Part I: The isotopic cloud model, *J. Atmos. Sci.*, *39*(6), 1323–1335.

Fischer, M. (2006), iCHASM, a flexible land-surface model that incorporates stable water isotopes, *Global Planet Change*, *51*(1–2), 121–130.

Gent, P., and J. McWilliams (1990), Isopycnal mixing in ocean circulation models, *J. Phys. Oceanogr.*, *20*(1), 150–155.

Gordon, C., C. Cooper, C. Senior, H. Banks, J. Gregory, T. Johns, J. Mitchell, and R. Wood (2000), The simulation of SST, sea ice extents and ocean heat transports in a version of the Hadley Centre coupled model without flux adjustments, *Clim. Dyn.*, *16*(2–3), 147–168.

Gregory, D., and D. Morris (1996), The sensitivity of climate simulations to the specification of mixed phase clouds, *Clim. Dyn.*, *12*(9), 641–651.

Gregory, D., and P. Rowntree (1990), A mass flux convection scheme with representation of cloud ensemble characteristics and stability-dependent closure, *Mon. Weather Rev.*, *118*(7), 1385–1406.

Gregory, J. M., P. A. Stott, D. J. Cresswell, N. A. Rayner, C. Gordon, and D. M. H. Sexton (2002), Recent and future changes in Arctic sea ice simulated by the HadCM3 AOGCM, *Geophys. Res. Lett.*, *29*(24), 2175, doi:10.1029/2001GL014575.

Hoffmann, G., M. Werner, and M. Heimann (1998), Water isotope module of the ECHAM atmospheric general circulation model: A study on timescales from days to several years, *J. Geophys. Res.*, *103*(D14), 16,871–16,896.

Hoffmann, G., et al. (2003), Coherent isotope history of Andean ice cores over the last century, *Geophys. Res. Lett.*, *30*(4), 1179, doi:10.1029/2002GL014870.

Johns, T. C., et al. (2003), Anthropogenic climate change for 1860–2100 simulated with the HadCM3 model under updated emissions scenarios, *Clim. Dyn.*, *20*(6), 583–612.

Joussaume, S., R. Sadourny, and J. Jouzel (1984), A general-circulation model of water isotope cycles in the atmosphere, *Nature*, *311*(5981), 24–29.

Jouzel, J. (1986), Multiphase and multistage condensation processes *Handbook of Environmental Isotope Geochemisty*, vol. 2, *The Terrestrial Environment*, pp. 61–112, Elsevier, New York.

Jouzel, J., and L. Merlivat (1984), Deuterium and oxygen 18 in precipitation: Modeling of the isotopic effects during snow formation, *J. Geophys. Res.*, *89*(D7), 11,749–11,757.

Jouzel, J., G. Russell, R. Suozzo, R. Koster, J. White, and W. S. Broecker (1987), Simulations of the HDO and $H_2{}^{18}O$ atmospheric cycles using the NASA GISS general circulation model: The seasonal cycle for present-day conditions, *J. Geophys. Res.*, *92*, 14,739–14,760.

Juillet-Leclerc, A., and G. Schmidt (2001), A calibration of the oxygen isotope paleothermometer of coral aragonite from Porites, *Geophys. Res. Lett.*, *28*(21), 4135–4138.

Latif, M., et al. (2001), Ensip: the El Nino simulation intercomparison project, *Clim. Dyn.*, *18*, 255–276.

Lee, J.-E., I. Fung, D. J. DePaolo, and C. C. Henning (2007), Analysis of the global distribution of water isotopes using the NCAR atmospheric general circulation model, *J. Geophys. Res.*, *112*, D16306, doi:10.1029/2006JD007657.

LeGrande, A. N., and G. A. Schmidt (2006), Global gridded data set of the oxygen isotopic composition in seawater, *Geophys. Res. Lett.*, *33*, L12604, doi:10.1029/2006GL026011.

LeGrande, A., G. Schmidt, D. Shindell, C. Field, R. Miller, D. Koch, G. Faluvegi, and G. Hoffmann (2006), Consistent simulations of multiple proxy responses to an abrupt climate change event, *Proc. Natl. Acad. Sci. U. S. A.*, *103*(4), 837–842.

Masson-Delmotte, V., et al. (2008), A review of Antarctic surface snow isotopic composition: observations, atmopsheric circulation and isotopic modelling, *J. Clim.*, *21*(13), 3359–3387, doi:10.1175/2007JCLI2139.1.

Mathieu, R., D. Pollard, J. E. Cole, J. W. C. White, R. S. Webb, and S. L. Thompson (2002), Simulation of stable water isotope variations by the GENESIS GCM for modern conditions, *J. Geophys. Res.*, *107*(D4), 4037, doi:10.1029/2001JD900255.

Merlivat, L., and J. Jouzel (1979), Global climatic interpretation of the deuterium-oxygen-18 relationship for precipitation, *J. Geophys. Res.*, *84*(8), 5029–5033.

Noone, D. (2008), The influence of midlatitude and tropical overturning circulation on the isotopic composition of atmospheric water vapor and Antarctic precipitation, *J. Geophys. Res.*, *113*, D04102, doi:10.1029/2007JD008892.

Noone, D., and I. Simmonds (2002), Associations between $\delta^{18}O$ of water and climate parameters in a simulation of atmospheric circulation for 1979–95, *J. Clim.*, *15*(22), 3150–3169.

Pardaens, A., H. Banks, J. Gregory, and P. Rowntree (2003), Freshwater transports in HadCM3, *Clim. Dyn.*, *21*(2), 177–195.

Pfirman, S., W. Haxby, H. Eicken, M. Jeffries, and D. Bauch (2004), Drifting Arctic sea ice archives changes in ocean surface conditions, *Geophys. Res. Lett.*, *31*, L19401, doi:10.1029/2004GL020666.

Pope, V., M. Gallani, P. Rowntree, and R. Stratton (2000), The impact of new physical parametrizations in the Hadley Centre climate model: HadAM3, *Clim. Dyn.*, *16*(2–3), 123–146.

Rozanski, K., L. Araguas-Araguas, and R. Gonfiantini (1992), Relation between long-term trends of oxygen-18 isotope composition of precipitation and climate, *Science*, *258*(5084), 981–985.

Schmidt, G. (1998), Oxygen-18 variations in a global ocean model, *Geophys. Res. Lett.*, *25*(8), 1201–1204.

Schmidt, G. A., G. Hoffmann, D. T. Shindell, and Y. Hu (2005), Modeling atmospheric stable water isotopes and the potential for constraining cloud processes and stratosphere-troposphere water exchange, *J. Geophys. Res.*, *110*, D21314, doi:10.1029/2005JD005790.

Schmidt, G. A., A. N. LeGrande, and G. Hoffmann (2007), Water isotope expressions of intrinsic and forced variability in a coupled ocean-atmosphere model, *J. Geophys. Res.*, *112*, D10103, doi:10.1029/2006JD007781.

Semtner, A. (2006), Model for thermodynamic growth of sea ice in numerical investigations of climate, *J. Phys. Oceanogr.*, *6*(3), 379–389.

Siegenthaler, U., and H. Oeschger (1980), Correlation of O-18 in precipitation with temperature and altitude, *Nature*, *285*(5763), 314–317.

Sime, L., D. Stevens, K. Heywood, and K. Oliver (2006), A decomposition of the Atlantic meridional overturning, *J. Phys. Oceanogr.*, *12*(36), 2253–2270.

Sime, L. C., J. C. Tindall, E. W. Wolff, W. M. Connolley, and P. J. Valdes (2008), Antarctic isotopic thermometer during a CO_2 forced warming event, *J. Geophys. Res.*, *113*, D24119, doi:10.1029/2008JD010395.

Smith, R. (1990), A scheme for predicting layer clouds and their water-content in a general-circulation model, *Q. J. R. Meteorol. Soc.*, *116*, 435–460.

Spencer, H., and J. Slingo (2003), The simulation of peak and delayed ENSO teleconnections, *J. Clim.*, *16*(11), 1757–1774.

Stewart, M. (1975), Stable isotope fractionation due to evaporation and isotopic exchange of falling waterdrops: Applications to atmospheric processes and evaporation of lakes, *J. Geophys. Res.*, *80*(9), 1133–1146.

Trenberth, K. (1997), The definition of El Nino, *Bull. Am. Meteorol. Soc.*, *78*(12), 2771–2777.

Tudhope, A., G. Shimmield, C. Chilcott, M. Jebb, A. Fallick, and A. Dalgleish (1995), Recent changes in climate in the far western equatorial Pacific and their relationship to the Southern Oscillation: Oxygen isotope records from massive corals, Papua New Guinea, *Earth Planet. Sci. Lett.*, *136*(3–4), 575–590.

Tudhope, A., C. Chilcott, M. McCulloch, E. R. Cook, J. Chappell, R. Ellam, D. Lea, J. Lough, and G. Shimmield (2001), Variability in the El Nino–Southern Oscillation through a glacial-interglacial cycle, *Science*, *291*(5508), 1511–1517.

Urban, F., J. Cole, and J. Overpeck (2000), Influence of mean climate change on climate variability from a 155-year tropical Pacific coral record, *Nature*, *407*(6807), 989–993.

Vuille, M., R. S. Bradley, R. Healy, M. Werner, D. R. Hardy, L. G. Thompson, and F. Keimig (2003), Modeling $\delta^{18}O$ in precipitation over the tropical Americas: 2. Simulation of the stable isotope signal in Andean ice cores, *J. Geophys. Res.*, *108*(D6), 4175, doi:10.1029/2001JD002039.

Werner, M., M. Heimann, and G. Hoffmann (2001), Isotopic composition and origin of polar precipitation in present and glacial climate simulations, *Tellus*, *53*(1), 53–71.

Zimmermann, U., D. Ehhalt, and K. Munnich (1967), Soil water movement and evapotranspiration change in the isotopic composition of water, in *Isotopes in Hydrology*, pp. 567–585, Int. At. Energy Agency, Vienna, Austria.

L. C. Sime, British Antarctic Survey, Cambridge CB3 0ET, UK.

J. C. Tindall and P. J. Valdes, Bristol Research Initiative for the Dynamic Global Environment, School of Geographical Sciences, University of Bristol, University Road, Bristol BS8 1SS, UK. (julia.tindall@bristol.ac.uk)